

Article

# Fast Power Reserve Emulation Strategy for VSWT Supporting Frequency Control in Multi-Area Power Systems

Ana Fernández-Guillamón <sup>1,\*</sup> , Antonio Viguera-Rodríguez <sup>2</sup> , Emilio Gómez-Lázaro <sup>3</sup>   
and Ángel Molina-García <sup>1</sup> 

<sup>1</sup> Department of Electrical Engineering, Universidad Politécnica de Cartagena, 30202 Cartagena, Spain; angel.molina@upct.es

<sup>2</sup> Department of Civil Engineering, Universidad Politécnica de Cartagena, 30203 Cartagena, Spain; aviguera.rodriguez@upct.es

<sup>3</sup> Renewable Energy Research Institute and DIEEAC-EDII-AB, Universidad de Castilla-La Mancha, 02071 Albacete, Spain; emilio.gomez@uclm.es

\* Correspondence: ana.fernandez@upct.es; Tel.: +34-968-325357

Received: 2 October 2018; Accepted: 11 October 2018; Published: 16 October 2018



**Abstract:** The integration of renewables into power systems involves significant targets and new scenarios with an important role for these alternative resources, mainly wind and PV power plants. Among the different objectives, frequency control strategies and new reserve analysis are currently considered as a major concern in power system stability and reliability studies. This paper aims to provide an analysis of multi-area power systems submitted to power imbalances, considering a high wind power penetration in line with certain European energy road-maps. Frequency control strategies applied to wind power plants from different areas are studied and compared for simulation purposes, including conventional generation units. Different parameters, such as nadir values, stabilization time intervals and tie-line active power exchanges are also analyzed. Detailed generation unit models are included in the paper. The results provide relevant information on the influence of multi-area scenarios on the global frequency response, including participation of wind power plants in system frequency control.

**Keywords:** frequency control; wind power integration; power system stability

## 1. Introduction

Traditionally, synchronous generators have provided frequency control reserves, which are released under power imbalance conditions to recover grid frequency [1]. In fact, any generation-demand imbalance leads the grid frequency to deviate from its nominal value, which can cause serious scale stability problems [2]. With the significant penetration of renewables, mainly wind power plants, a proportional capacity of the system reserves must be provided by these new resources [3]. In this way, reference [4] considers that wind power plant participation in grid frequency control is imminent. However, wind turbines usually include back-to-back converters, and they are electrically decoupled from the grid through power electronic converters [5]. Consequently, with the significant integration of wind power into power systems, grid frequency tends to degrade progressively due to the reduction of the grid inertial responses [6]. Therefore, this new scenario presents a preliminary reduction of reserves from conventional generation units, mainly in weak and/or isolated power systems with high renewable resource penetration [7,8]. Moreover, these problems would be exacerbated in micro-grids, with a high share of power-electronically interfaced and thus a low grid inertia [9,10]. Under this framework, frequency control strategies must be included in wind power plants to provide additional

active power under disturbances [11]. These new strategies would allow us to integrate Variable Speed Wind Turbines (VSWTs) into these services, replacing conventional power plants by renewables [12] and maintaining a reliable power system operation [13]. Most of the proposed strategies for VSWTs are based on ‘hidden inertia emulation’, enhancing their inertia response [14–16]. According to the specific literature, ‘Fast power reserve emulation’ has been proposed as a suitable solution. It is based on supplying the kinetic energy stored in the rotating masses to the grid as an additional active power, being subsequently recovered through an under-production period (recovery) [17–19]. Different studies can be found to discuss the definition of overproduction period and the transition from overproduction to recovery period [20–25]. These studies are mainly focused on analyzing the inertia reduction problem on isolated power systems [20,21,23–27]. However, there is a lack of contributions focused on large interconnected power systems with high wind power penetration [28]. These new scenarios are in line with current wind generation units, covering more than 20% in different power systems. Moreover, renewables have accounted for more than 50% at different times in some European countries such as Spain, Portugal, Ireland, Germany or Denmark [29].

In general, synchronous generators inherently release or absorb kinetic energy as an inertial response to imbalance situations [24]. However, to recover the grid frequency at the nominal value, an additional control system is needed as well [30]. Automatic Generation Control (AGC) is thus considered as one of the most important ancillary services in power systems. AGC is used to match the total generation with the total demand, including power system losses [31]. Over the last decade, different authors have proposed several control strategies and optimization techniques. A modified AGC for an interconnected power system in a deregulated environment is described in [32]. A similar contribution can be found in [33], where an energy storage system is added to a multi-area power system, and the  $I$  controller gains are optimized by using the Opposition-based Harmony Search algorithm. A teaching-learning process based on an optimization algorithm to tune both  $I$  and  $PID$  controller parameters in single and multi-area power systems is described in [34]. In [35], a hybrid fuzzy PI controller is proposed for AGC of multi-area systems, yielding significant improvements compared to previous approaches. In [36], the gray wolf optimization method is proposed to tune the controller gains of an interconnected power system. This solution presented a more suitable tuning capability than other population-based optimization techniques. An optics inspired optimization algorithm is proposed in [37] and compared to other optimization algorithms, reaching a better performance for maximum overshoot and settling time values. However, in these contributions, only thermal, gas and hydro-power plants are considered from the supply side [32–36]. Therefore, multi-area power system modeling by including wind power plants are required to simulate frequency excursions under power imbalance conditions. Consequently, and by considering previous contributions, this paper analyzes different power imbalance situations and the corresponding frequency deviations in a multi-area interconnected power system with high wind power penetration. The main contributions of the paper are summarized as follows:

- Different multi-area power systems are analyzed with significant wind power integration, in line with current shares of renewables accounting for between 25% and 40%. Most previous studies on multi-area power systems only consider conventional generating units, such as thermal, gas and hydro-power [38–41].
- Wind power plants include a fast power reserve emulation control strategy in order to provide frequency response under power imbalances. Indeed, there is a lack of contributions describing frequency control response in wind power plants without energy storage solutions under multi-area power systems [42–45].
- The total power exchanged between areas is in line with the recent EU-wide targets, assuming a power interconnection share of 10% [46].
- The impact of wind power plants located in different areas on the frequency evolution is included in our model and discussed in detail.

The rest of the paper is organized as follows: Section 2 presents the frequency control strategy for VSWTs. The implemented multi-area interconnected power system is described in Section 3. The results are provided and widely discussed in Section 4. Finally, the conclusions are presented in Section 5.

## 2. Improving Frequency Control Strategy of Wind Turbines

According to the specific literature, different methods for VSWTs have been proposed to provide frequency control. Figure 1 summarizes the corresponding solutions to be implemented in wind power plants: (i) de-loading, (ii) droop control and (iii) inertial response [47]. With regard to de-loading control methods, they are based on operating VSWTs below their optimal generation point. A certain amount of active power reserve is thus available to supply additional generation under a contingency [48]. It can be implemented by regulating the pitch angle from  $\beta_{min}$  to a maximum value or by increasing the rotational speed above the Maximum Power Point Tracking (MPPT) speed (over-speeding) [49]. An extension of de-loading strategy applied to Photovoltaic system (PV) taking into account a percentage of the PV power production for back-up reserve can be found in [50]. Secondly, droop control solutions have a significant influence on the frequency minimum value (nadir) and the frequency recovery [51]. The controller is based on considering the torque/power-set point as a function of the frequency excursion ( $\Delta f$ ) and the rate of change of frequency (ROCOF) [52–56]. Finally, ‘hidden inertia’ controllers introduce a supplementary loop into the active power control. This additional loop control is only added under frequency deviations. Both blades and rotor inertia are then used to provide primary frequency response. Different approaches can be found in the specific literature. One solution is based on emulating similar inertia response to conventional generation units, shifting the torque/power reference proportionally to the ROCOF [51,57–60]. Another study uses the fast power reserve emulation. Constant overproduction power is released from the kinetic energy stored in the rotating mass of the wind turbine, with the rotational speed being recovered later through an underproduction period [17,20,21,25,47,61].

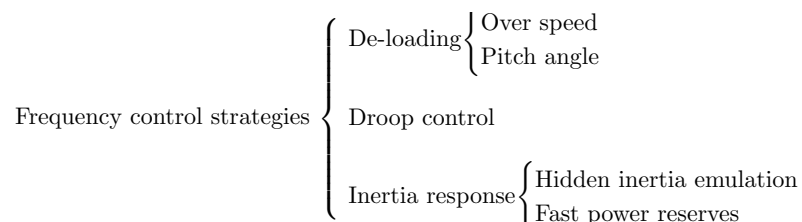


**Figure 1.** Wind power plant frequency control: general overview [28,47].

In line with previous contributions, the frequency control strategy for VSWTs implemented in this work is based on the fast power reserve emulation technique developed by the authors in [25]. This approach improves an initial proposal described in [61], by minimizing frequency oscillations and smoothing the wind power plant frequency response. Three operation modes are considered: normal operation mode, overproduction mode and recovery mode, see Figure 2. Different active power ( $P_{cmd}$ ) values are determined aiming to restore the grid frequency under power imbalance conditions. Figure 2b depicts the VSWTs active power variations ( $\Delta P_{WF}$ ) submitted to an under-frequency excursion, being  $\Delta P_{WF} = P_{cmd} - P_{MPPT}(\Omega_{MPPT})$ .

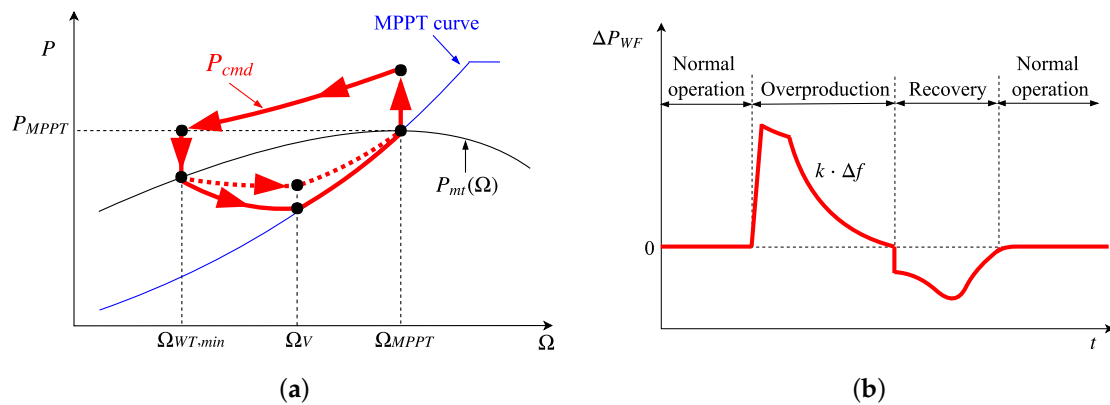


**Figure 2.** Wind frequency control strategy and VSWTs’ active power variation ( $\Delta P_{WF}$ ) [25]; (a) frequency control strategy used for VSWTs; (b)  $\Delta P_{WF}$  with frequency control strategy.

1. *Normal operation mode.* The VSWTs operate at a certain active power value ( $P_{cmd}$ ), according to the available mechanical power for a specific wind speed,  $P_{mt}(\Omega_{WT})$ . It matches the maximum available active power for this current wind speed  $P_{MPPT}(V_W)$ ; see Figure 2a,

$$P_{cmd} = P_{mt}(\Omega_{WT}) = P_{MPPT}(V_W). \tag{1}$$

Under power imbalance conditions, and assuming an under-frequency deviation, the frequency controller strategy changes to the overproduction mode and, subsequently,  $\Delta f < -\Delta f_{lim} \rightarrow$  Overproduction.

2. *Overproduction mode.* The active power supplied by the VSWTs involves (i) mechanical power  $P_{mt}$  available from the  $P_{mt}(\Omega_{WT})$  curve and (ii) additional active power  $\Delta P_{OP}$  provided by the kinetic energy stored in the rotational masses,

$$P_{cmd} = P_{mt}(\Omega_{WT}) + \Delta P_{OP}(\Delta f). \tag{2}$$

$\Delta P_{OP}$  is estimated proportionally to the evolution of frequency excursion in order to emulate primary frequency control of conventional generation units [26,62]. Most previous approaches assume  $\Delta P_{OP}$  as a constant value independent of the frequency excursion [22,23,61]. Moreover, the mechanical power  $P_{mt}$  is also considered as constant by most authors, even when rotational speed decreased [20–24,61]. This overproduction strategy remains active until one of the following conditions is met: the frequency excursion disappears, the rotational speed reaches a minimum allowed value, or the commanded power is lower than the maximum available active power,

$$\left. \begin{aligned} \Delta f &> -\Delta f_{lim} \\ \Omega_{WT} &< \Omega_{WT,min} \\ P_{cmd} &< P_{MPPT}(\Omega_{MPPT}) \end{aligned} \right\} \rightarrow \text{Recovery}. \tag{3}$$

3. *Recovery mode.* With the aim of minimizing frequency oscillations, wind power plants have to move from overproduction mode to recovery mode as smoothly as possible, avoiding abrupt power changes and, subsequently, undesirable secondary frequency shifts [20,22,24,61]. With this aim, the authors’ solution described in [25] follows the mechanical power curve  $P_{mt}(\Omega_{WT})$  according to the wind speed instead of the maximum power curve  $P_{MPPT}(\Omega_{WT})$  [22]. The power provided by the VSWTs in this mode is based on two periods according to [25]: (i) a parabolic trajectory and (ii) following the  $P_{MPPT}$  curve proportional to the difference between  $P_{mt}(\Omega_{WT})$  and  $P_{MPPT}(\Omega_{WT})$ . The normal operation mode then can be recovered when either  $\Omega_{MPPT}$  or  $P_{MPPT}(\Omega_{MPPT})$  are respectively reached by the wind turbine.

This strategy was evaluated in [25] and compared to [61] for single-area power system modeling, providing an improved frequency response under power imbalance conditions. This approach is considered in the present paper and extended to a multi-area power system with significant wind power integration into different areas.

### 3. Power System Modeling

#### 3.1. General Overview

Traditional power system modeling for frequency deviation analysis under imbalance conditions is usually based on the following expression [63],

$$\Delta f = \frac{1}{2 H_{eq} s + D_{eq}} \cdot (\Delta P_g - \Delta P_L), \quad (4)$$

where  $\Delta f$  is the frequency variation from nominal system frequency,  $H_{eq}$  is the equivalent inertia constant of the system,  $D_{eq}$  is the equivalent damping factor of the loads, and  $\Delta P_g - \Delta P_L$  is the power imbalance.  $H_{eq}$  is estimated from Equation (5),  $H_m$  is the inertia constant of  $m$ -power plant,  $S_{B,m}$  is the rated power of the  $m$ -generating unit, CG is the total number of conventional synchronous generators and  $S_B$  is the base power system:

$$H_{eq} = \frac{\sum_{m=1}^{CG} H_m \cdot S_{B,m}}{S_B}. \quad (5)$$

Transmission level voltage is usually considered for multi-area interconnection purposes through tie-lines. Frequency and tie-line power exchange can vary according to variations in power load demand [64–68]. The total tie-line power exchange between two areas is determined by

$$\Delta P_{tie_{i,j}} = \frac{2 \cdot \pi \cdot T_{i,j}}{s} \cdot (\Delta f_i - \Delta f_j), \quad (6)$$

where  $T_{i,j}$  is the synchronizing moment coefficient of the tie-line between  $i$  and  $j$  areas.

When a frequency deviation is detected, the balance between an interconnected power system is determined by generating the Area Control Error signal ( $ACE$ ), expressed as a linear combination of the tie-line power exchange and the frequency deviation [69]

$$ACE_i = B_i \cdot \Delta f_i + \sum_{\substack{j=1 \\ j \neq i}}^N \Delta P_{tie_{i,j}}, \quad (7)$$

where  $i, j$  refers to  $i$  and  $j$  areas, respectively,  $B$  is the bias-factor,  $\Delta P_{tie}$  is the variation in the exchanged tie-line power and  $N$  is the total number of interconnected areas. Figure 3 schematically shows these power exchanges for a three-area power system example. Recent contributions focused on a new control logic of the Balancing Authority Area Control Error Limit (BAAL) Standard adopted in the North American power grid can be found in [70].

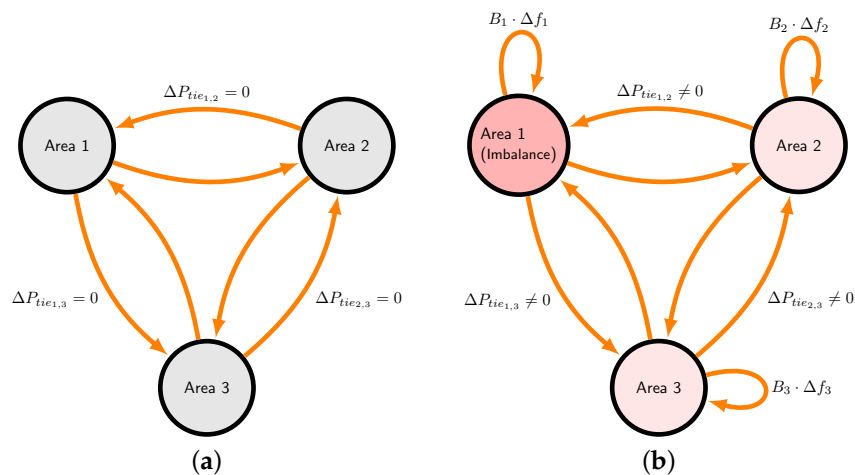


**Figure 3.** Multi-area power system. (a) balanced situation; (b) imbalanced situation in Area 1.

### 3.2. Supply-Side Modeling

From the supply-side, the power systems considered for simulation purposes involve conventional generating units (such as non-reheat thermal and hydro-power) and renewable energy sources (wind and PV power plants). One equivalent generator is used for each type of production to model the supply-side. This assumption is in line with previous contributions focused on frequency strategy control analysis.

The conventional generating unit models considered for simulations can be seen in Figure 4. Taking into account the specific literature, they are modeled according to the simplified governor-based models widely used and proposed in [62]. Parameters are provided in Tables 1 and 2, respectively. The different transfer functions of governor and turbine are indicated in Figure 4.

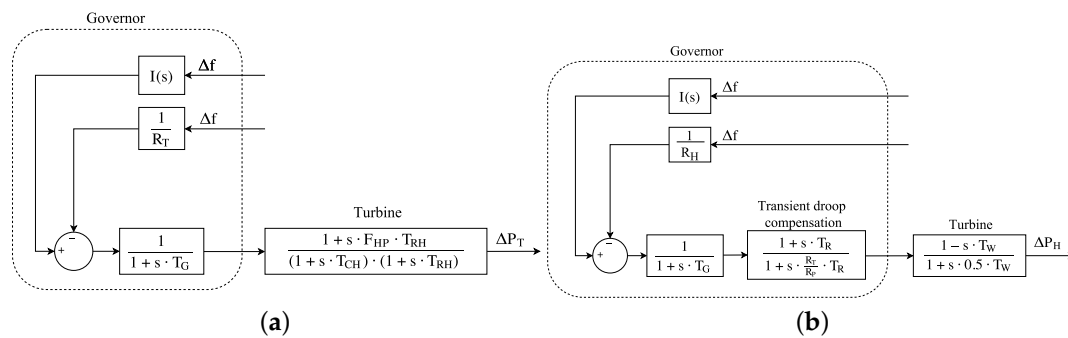


**Figure 4.** Conventional generation modeling. (a) thermal plant model; (b) hydro-power plant model.

**Table 1.** Thermal power plant parameters [62].

Parameter	Name	Value (pu <sub>thermal</sub> )
$T_G$	Speed relay pilot valve	0.20
$F_{HP}$	Fraction of power generated by high pressure section	0.30
$T_{RH}$	Time constant of reheater	7.00
$T_{CH}$	Time constant of main inlet volumes and steam chest	0.30
$R_T$	Speed droop	0.05
$I(s)$	Integral controller	1.00
$H_{thermal}$	Inertia constant	5.00 s

**Table 2.** Hydro-power plant parameters [62].

Parameter	Name	Value (pu <sub>hydro</sub> )
$T_G$	Speed relay pilot valve	0.20
$T_R$	Reset time	5.00
$R_T$	Temporary droop	0.38
$R_P$	Permanent droop	0.05
$T_W$	Water starting time	1.00
$R_H$	Speed droop	0.05
$I(s)$	Integral controller	1.00
$H_{hydro}$	Inertia constant	3.00 s

Wind power plants are able to provide frequency response according to the strategy discussed in Section 2. An aggregated model for wind power plants is considered for the simulation purposes. They are represented by one equivalent generator, which is generally accepted in the specific literature for frequency response simulations (Figure 5). The equivalent wind turbine has  $n$ -times the size of each individual wind turbine, with  $n$  being the number of wind turbines [71,72]. The equivalent wind turbine model is based on [73,74], which have been widely used in recent publications [22,23,25,75–77]. Parameters are shown in Table 3. The remaining renewable generation is modeled through an equivalent PV power plant connected to the grid. It represents a renewable non-dispatchable energy source, following recent contributions [78]. Due to the short period of simulated time (under 5 min), a constant active power provided by this non-dispatchable resource is considered for our analysis.

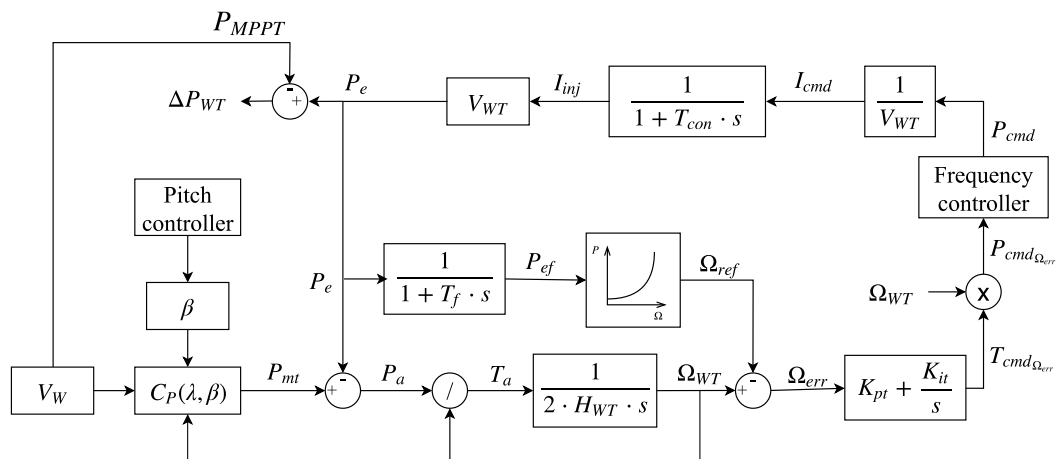


**Figure 5.** Aggregated wind power plant model with frequency controller.

**Table 3.** Wind turbine parameters [74].

Parameter	Name	Value
$V_w$	Wind speed	10 m/s
$S_n$	Rated power	3.6 MW
$H_{WT}$	Inertia constant	5.19 s
$\Omega_0$	Base rotational speed	1.335 rad/s
$T_f$	Time delay to measure electric power	5 s
$T_{con}$	Time delay to generate the injected current $I_{inj}$	0.020 s
$V_{WT}$	Wind turbine voltage	1 pu <sub>WT</sub>
$K_{pt}$	Proportional constant of speed controller	3 pu <sub>WT</sub>
$K_{it}$	Integral constant of speed controller	0.6 pu <sub>WT</sub>

### 3.3. Area Descriptions

Figure 6 summarizes the percentages for the different generating units of each area. Previous studies address the problem of multi-area power systems considering only conventional power plants (mainly thermal, hydro-power and gas) and assuming two or three areas [32–36,38–41]. In this work, two different interconnected multi-source power systems are analyzed: (i) a two-area power system (considering only Areas 1 and 2) and (ii) a three-area power system. Both systems allow us to study in detail the relationships between the number of areas and the exchanged power between them when a significant number of renewable energies are considered from the supply-side. A base power of 2000 MW per area is assumed that corresponds to the capacity of each area. In Europe, it is expected that wind and PV will cover up to 30% and 18% of the demand respectively by 2030 [79,80]. Therefore, the integration of these sources in the areas considered in this paper are in line with current European road-maps, having a RES/non-dispatchable integration lying between 25% to 50%. In addition,  $\Delta P_{tie_{i,j}}$  is limited to a maximum value of 10%. This limit agrees with recent EU-wide targets, which expect to have an interconnection power of 10% in the year 2020 [46]. Most contributions found in the literature review either do not limit the maximum tie-line power, or it is not indicated [81–84].

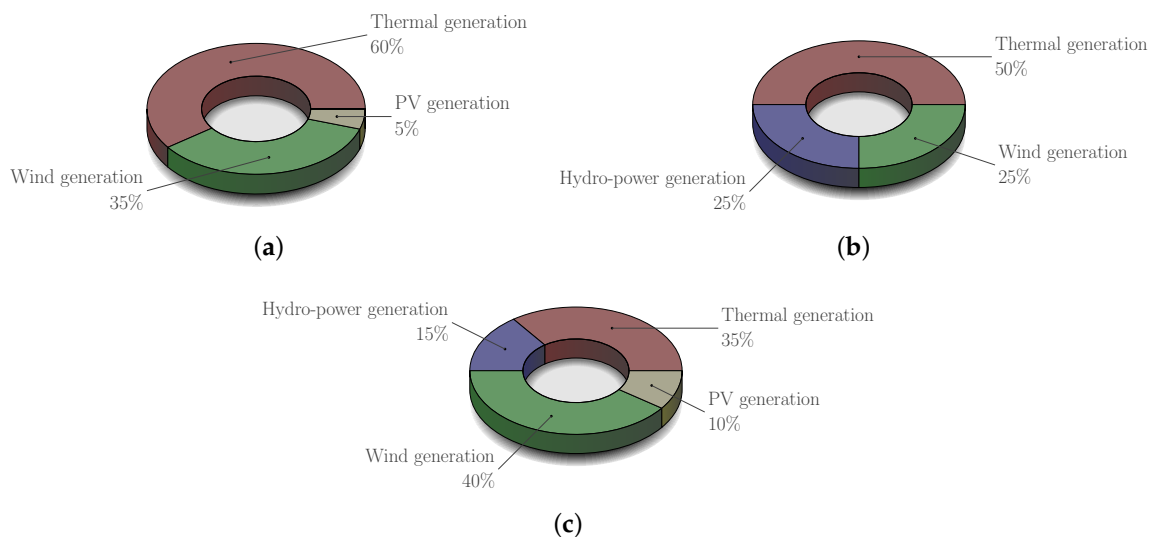


**Figure 6.** Generation contribution per area. (a) Area 1; (b) Area 2; (c) Area 3.

$T_{i,j}$  and  $B$  values are provided in Table 4 for the two-interconnected areas [30,35] and in Table 5 for three-interconnected areas [30]. The equivalent inertia  $H_{eq}$  of each area is calculated according to Equation (5), and taking into account the inertia constants of thermal and hydro-power plants indicated in Section 3.2. With regard to the damping factor, the impact of an inaccurate value is relatively small if the power system is stable [85]. Moreover, it is expected to decrease accordingly to the use of variable frequency drives [86]. Table 6 summarizes different values proposed for the damping factor in the literature over recent decades. A value of  $D_{eq} = 1$  is considered for simulation purposes, which is in line with recent contributions and is lower than values corresponding to previous works. A general overview of a two-area power system can be seen in Figure 7.

**Table 4.** Interconnected two-area power system parameters [30,35].

Parameter	Name	Value
$B_1$	Bias factor of Area 1	0.425
$B_2$	Bias factor of Area 2	0.425
$T_{1,2}$	Synchronizing moment coefficient between Areas 1 and 2	0.545
$H_{eq,1}$	Equivalent inertia constant of Area 1	2.997 s
$H_{eq,2}$	Equivalent inertia constant of Area 2	3.324 s

**Table 5.** Interconnected three-area power system parameters [30].

Parameter	Name	Value
$B_1$	Bias factor of Area 1	0.3483
$B_2$	Bias factor of Area 2	0.3827
$B_3$	Bias factor of Area 3	0.3629
$T_{1,2}$	Synchronizing moment coefficient between Areas 1 and 2	0.2
$T_{2,3}$	Synchronizing moment coefficient between Areas 2 and 3	0.12
$T_{3,1}$	Synchronizing moment coefficient between Areas 3 and 1	0.25
$H_{eq,1}$	Equivalent inertia constant of Area 1	2.997 s
$H_{eq,2}$	Equivalent inertia constant of Area 2	3.324 s
$H_{eq,3}$	Equivalent inertia constant of Area 3	2.246 s

**Table 6.** Damping factor values.

Ref.	Value (pu/Hz)	Analysis	Year
[62]	1–2	Power system stability	1994
[87]	0.83	Two areas with non-reheat thermal units	2011
[88]	1.66	Two areas with thermal units	2011
[89]	1–1.8	Three areas with non-reheat thermal units	2012
[90]	2	One area with nuclear, thermal, wind and PV	2012
[91]	0.5–0.9	Three areas with nonlinear thermal units	2013
[92]	0.83	Two areas non-reheat thermal units	2013
[93]	0.83	Two areas with thermal units	2013
[67]	0.83	Two areas with reheat units	2015
[94]	0.8	IEEE 9 bus system with hydro-power, gas and wind turbines	2016
[95]	1–1.8	One and three areas with non-reheat thermal units	2017
[96]	1–1.8	Three areas with non-reheat thermal units	2018
[97]	1	Two areas with non-reheat thermal units	2018

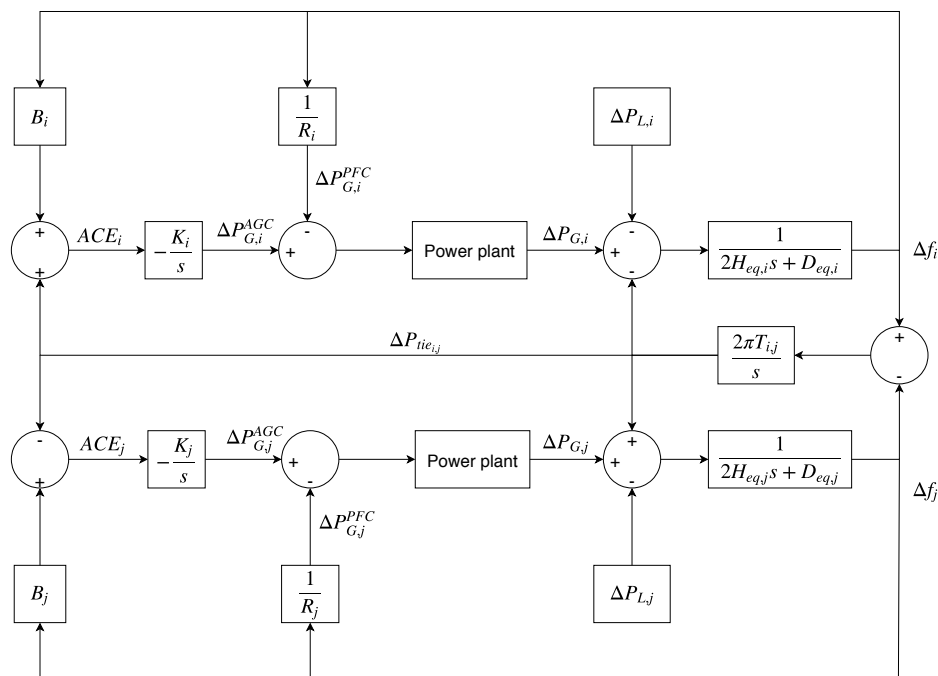


**Figure 7.** Two-area power system modeling for frequency control.

### 4. Results

As was discussed in Section 3, and with the aim of evaluating frequency oscillations and power system performances under imbalance conditions with different number of areas, two different

multi-area power systems were simulated: (i) a two-area power system and (ii) a three-area power system. Both power systems were implemented in Matlab/Simulink© (2016, MathWorks, Natick, MA, USA). Source codes are available under request.

#### 4.1. Two-Area Interconnected Power System

Firstly, and in order to evaluate the sensitivity of frequency excursions in a multi-area power system, two different imbalance conditions were simulated. In both cases, one area is submitted to imbalances while the other area maintains a balanced condition. A 5% increase in demand of the base power is assumed in all simulations as imbalance power ( $\Delta P_{L,1} = \Delta P_{L,2} = 100$  MW). Under these scenarios, with an active-power deficit, different frequency control strategies are addressed by the simulations depending on the generation units involved in the frequency response: *case* (1) whole conventional generation units of the multi-area power system; *case* (2) whole conventional generation units and only wind power plants within the area submitted to imbalances; and *case* (3) whole conventional generation units and wind power plants.

Figure 8a,b shows the frequency oscillations in both areas when a power imbalance is applied to Area 1 ( $\Delta P_{L,1}$ ). As can be seen, the maximum nadir is achieved in both areas when *case* (1) is conducted. The nadir values are improved when wind power plants are considered for frequency control: *cases* (2) and (3). Indeed, *case* (2) offers a smoother and less oscillatory response than *case* (3), yielding a stabilization time interval very similar to *case* (1). Moreover, *case* (3) causes three different well-identified frequency shifts: the first one is due to the power imbalance; the second one occurs due to the lack of coordination between power plants as well as the different time response of the supply-side operation units (see Figure 9); and the last one depends on the transition from overproduction mode to recovery mode of the wind power plant located in Area 2 (see Figure 2b and the active power decrease in WPP2 Figure 9).

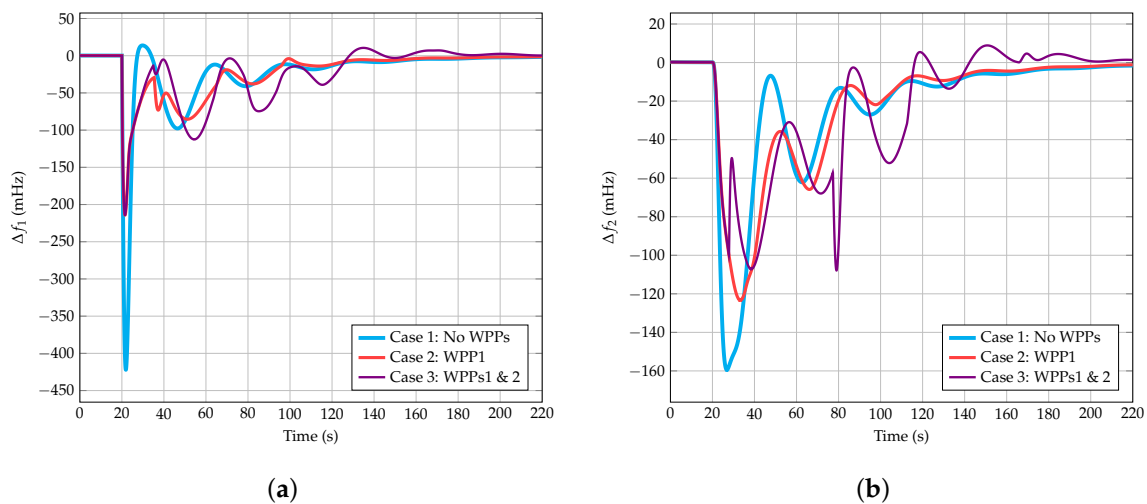


**Figure 8.** Area 1 under power imbalance ( $\Delta P_{L,1}$ ); (a) frequency oscillations in Area 1; (b) frequency oscillations in Area 2.

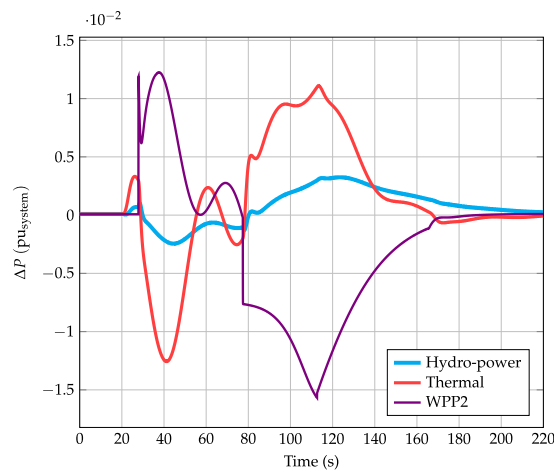


Figure 9. Area 1 under power imbalance ( $\Delta P_{L,1}$ ): generation deviations in Area 2.

A similar study can be carried out by considering power imbalance conditions in Area 2 ( $\Delta P_{L,2}$ ). Figure 10 compares the results in terms of nadir for both scenarios ( $\Delta P_{L,1}$  and  $\Delta P_{L,2}$ ) and considering the different frequency control strategies. As can be seen, minor differences are found in both analyses. In addition, Figure 11 compares the tie-line power evolution under both imbalance conditions,  $\Delta P_{L,1}$  and  $\Delta P_{L,2}$  accordingly, and peak-to-peak tie-line power exchange. Subsequently, and according to the generation mix considered in each area, frequency oscillations and active tie-line power results present similar values regardless of the area submitted to imbalances. Based on these results, and taking into account the different frequency control strategies implemented and simulated, lower frequency oscillations are obtained when only wind power plants within the area submitted to imbalance conditions are considered. Therefore, the contribution of wind power plants from other areas under frequency excursions would provide additional oscillation responses.

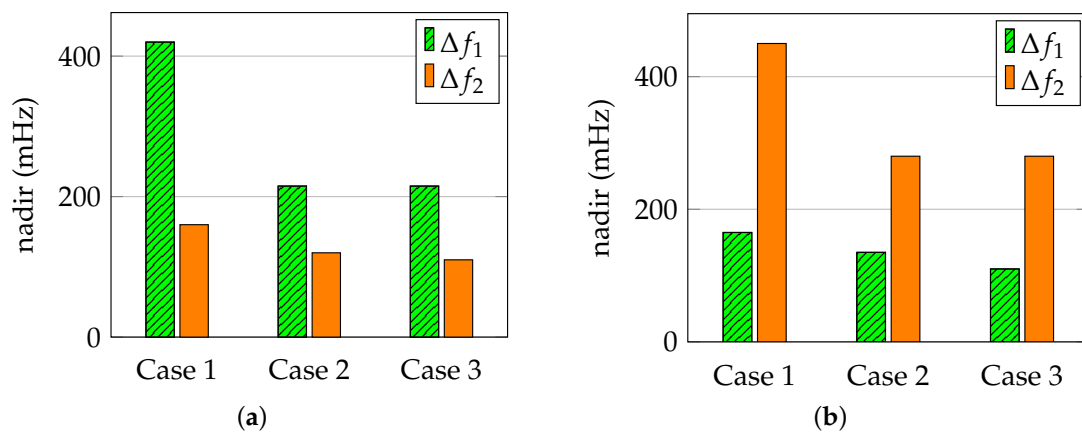
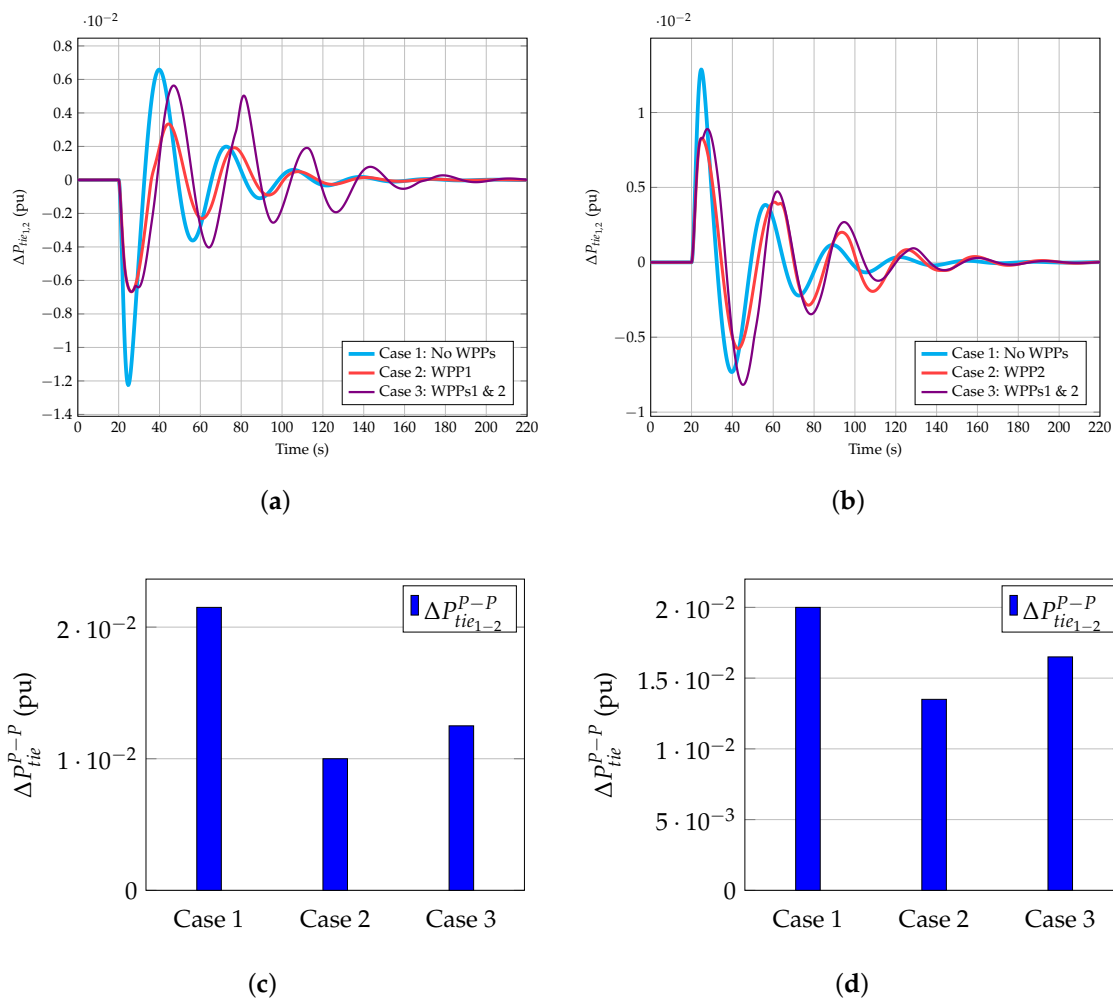


Figure 10. Nadir: Comparison of  $\Delta P_{L,1}$  and  $\Delta P_{L,2}$  scenarios. (a) Area 1 submitted to imbalance ( $\Delta P_{L,1}$ ); (b) Area 2 submitted to imbalance ( $\Delta P_{L,2}$ ).

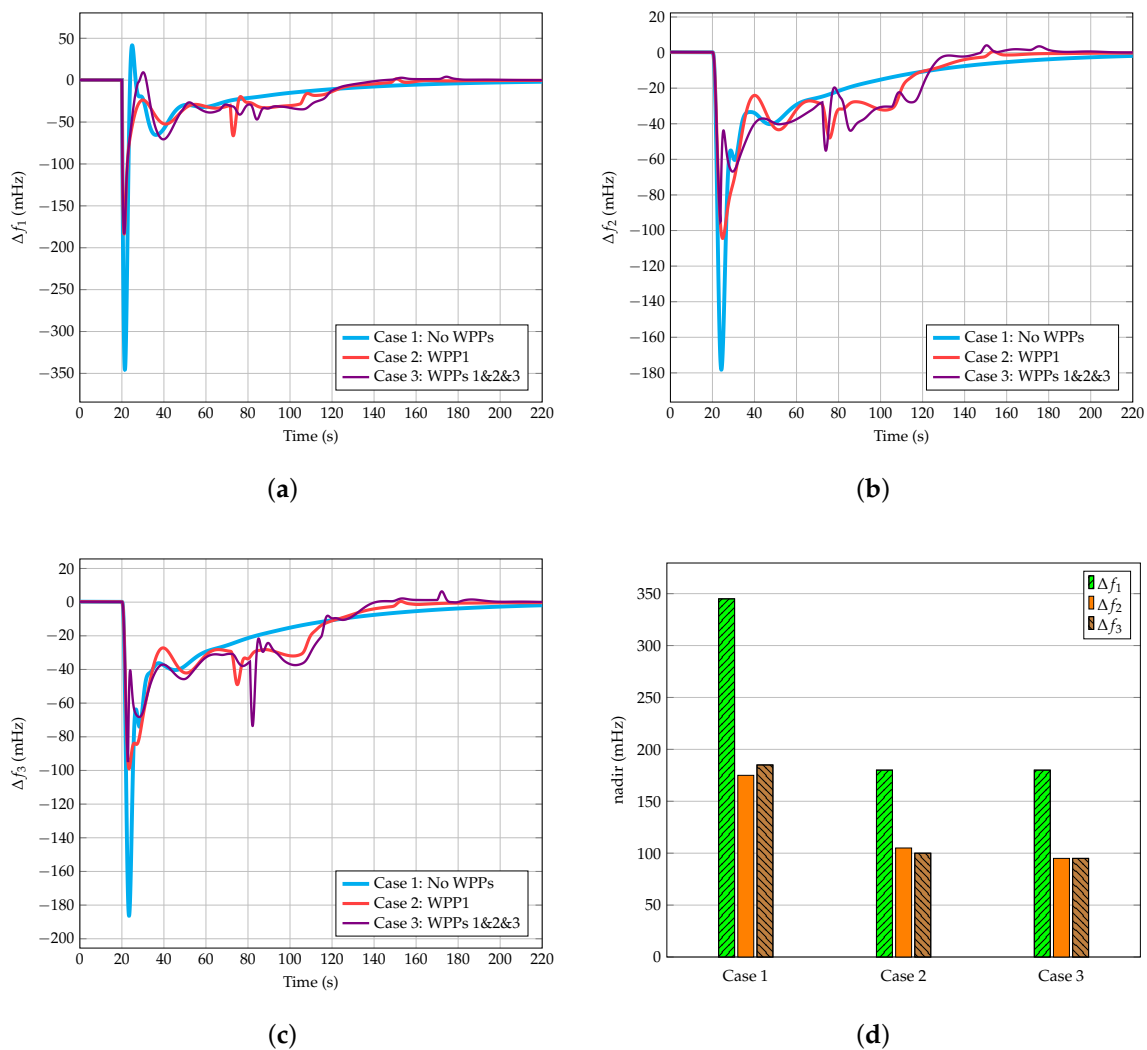


**Figure 11.** Active tie-line power evolution: comparison of  $\Delta P_{L,1}$  and  $\Delta P_{L,2}$  scenarios. (a) Area 1 submitted to power imbalance ( $\Delta P_{L,1}$ ); (b) Area 2 submitted to power imbalance ( $\Delta P_{L,2}$ ); (c) Area 1 submitted to imbalance ( $\Delta P_{L,1}$ ); (d) Area 2 submitted to imbalance ( $\Delta P_{L,2}$ ).

#### 4.2. Three-Area Interconnected Power System

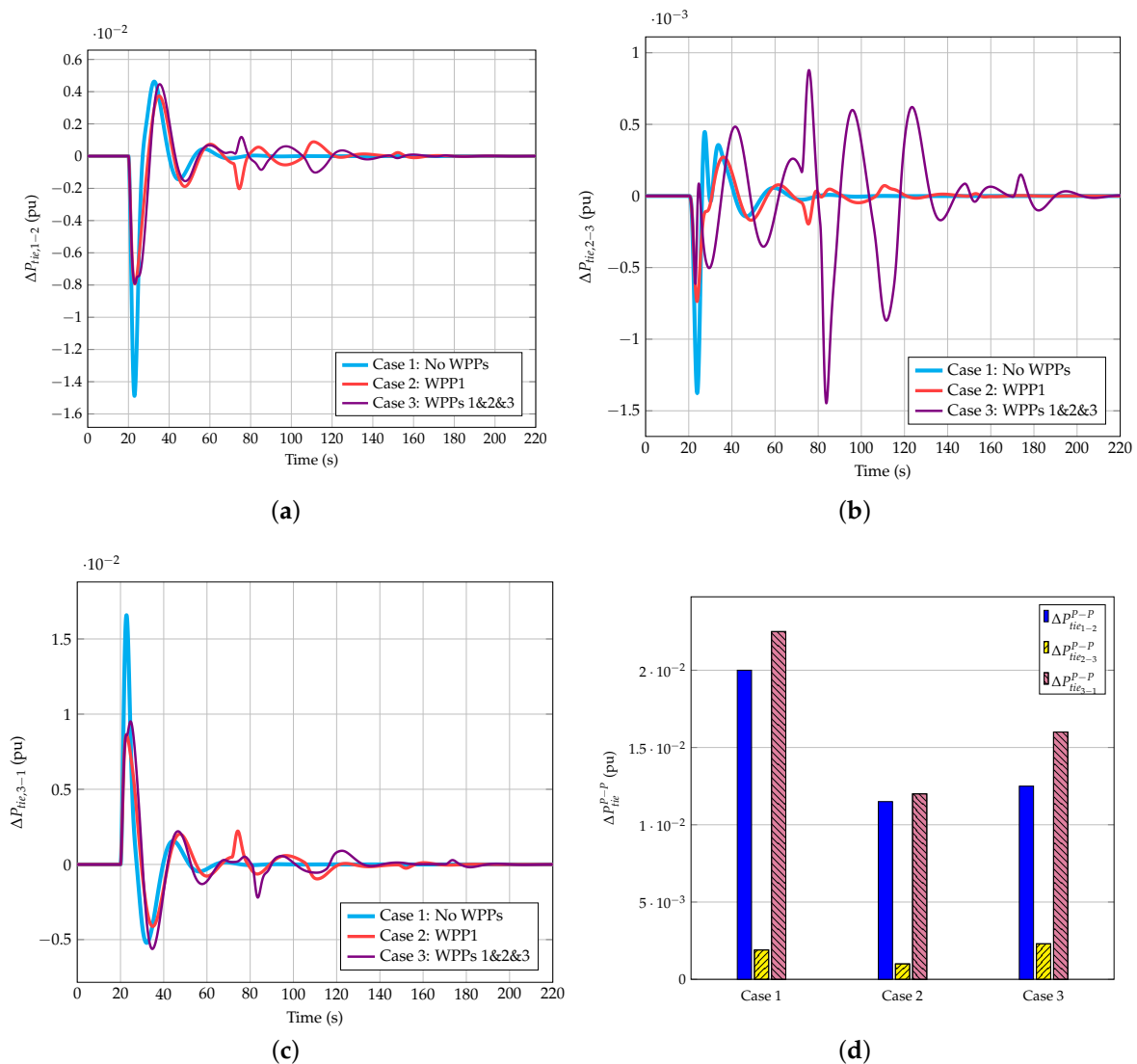
Considering the preliminary conclusion given in Section 4.1, where similar results are obtained independently of the area submitted to imbalances, the authors reduce the number of simulations in this three-area interconnected power system, assuming only that one area is submitted to imbalance conditions. Different frequency control strategies are then simulated by including an active-power deficit applied to Area 1,  $\Delta P_{L,1}$ . It is also defined as a step of 5% with respect to the base power ( $\Delta P_{L,1} = 100$  MW).

Figure 12 depicts the frequency deviation of each area and the nadir comparison according to the different frequency control strategies. As can be seen, the results are in line with those obtained previously, when a two-area power system was considered. Therefore, the maximum nadir values are obtained in all areas when wind power plants are not included for frequency control. When wind power plants provide frequency response, the nadir values of all areas are considerably improved. Regarding case (2) and case (3), nadir values give similar results. However, larger frequency oscillations are identified when case (3) is conducted, especially in Area 2 and area 3. This behavior is a consequence of the wind power variations due to the different operation modes of each frequency controller, increasing the tie-line power exchanged between these two areas. Stabilization time presents similar values ( $t_{stab} \simeq 100$  s) in all cases and areas.



**Figure 12.** Frequency oscillations: Area 1 under power imbalance ( $\Delta P_{L,1}$ ); (a) frequency oscillations in Area 1 ( $\Delta f_1$ ); (b) frequency oscillations in Area 2 ( $\Delta f_2$ ); (c) frequency oscillations in Area 3 ( $\Delta f_3$ ); (d) nadir values: case comparison.

Figure 13 shows and compares the tie-line power variation and its peak-to-peak value. As can be seen, tie-line power exchange does not overcome the maximum restriction of 10% under any circumstances. Power exchanged between areas 2–3 is practically negligible regardless of the frequency control strategy, as the frequency deviations in these areas are a consequence of imbalances subsequently induced by Area 1 (see Section 3.1). As was previously mentioned, with the use of the wind power plants in all the areas  $\Delta P_{tie_{2,3}}$  increases due to the wind power plants variations. Actually,  $\Delta P_{tie_{2,3}}$  case (3) doubles the value of case (2), subsequently producing more oscillations in frequency deviations in those areas, as depicted in Figure 12. Therefore, case (2) is suggested by the authors under imbalance conditions to reduce frequency oscillations and power flow between areas.



**Figure 13.** Area 1 under power imbalance ( $\Delta P_{L,1}$ ): tie-line power comparison; (a) tie-line power variation between Areas 1 and 2; (b) tie-line power variation between Areas 2 and 3; (c) tie-line power variation between Areas 3 and 1; (d) comparison among peak-to-peak tie-line power variation exchange.

## 5. Conclusions

Multi-areas interconnected power systems are analyzed under power imbalance conditions and with high wind energy integration. From the supply-side, conventional and renewable resources are considered, including thermal, hydro-power, wind and PV power plants. Wind power integration accounts for between 25% and 40%, corresponding to current percentages in some European countries. Tie-line power is limited to a maximum value of 10%, in line with recent EU directives. Different cases are compared and analyzed, depending on frequency control strategies applied by wind power plants. According to the results, frequency responses are improved by including wind power plants in frequency control, in comparison with simulations where this task is only performed by conventional generation units. Of the different cases, the nadir reductions are maximized when only wind power plants within the area submitted to imbalances are considered. In this case, the nadir is reduced between 40% and 50% in the area submitted to imbalanced areas in comparison to conventional generational unit scenarios. Moreover, these nadir values are also reduced in the other areas between 20% and 30%. When wind power responses of all areas are considered, higher frequency oscillations and lower nadir reductions can be reached in comparison with only conventional generation unit

scenarios. Stabilization time remains almost constant under different situations, and very similar to simulations where only conventional units respond under frequency excursions. Subsequently, the authors suggest including only wind power plant frequency response within the area submitted to imbalances, avoiding additional frequency oscillations coming from wind power plants located in the other areas.

**Author Contributions:** Data curation, A.F.-G.; formal analysis, A.F.-G.; methodology, A.F.-G., A.V.-R. and A.M.-G.; software, A.F.-G.; supervision, A.V.-R. and E.G.-L.; visualization, A.M.-G.; writing—original draft, A.M.-G.; writing—review & editing, E.G.-L.

**Funding:** This work was supported by ‘Ministerio de Educación, Cultura y Deporte’ of Spain (ref. FPU16/04282). The authors are grateful for the financial support from the Spanish Ministry of the Economy and Competitiveness and the European Union —ENE2016-78214-C2-2-R.

**Conflicts of Interest:** The authors declare no conflict of interest.

## Abbreviations

The following abbreviations are used in this manuscript:

$ACE$	Area Control Error
$AGC$	Automatic Generation Control
$CG$	Total number of conventional synchronous generators
$ROCOF$	Rate of Change of Frequency
$VSWTs$	Variable Speed Wind Turbines
$WPP$	Wind Power Plant
$nadir$	Minimum value of the frequency excursion
$n$	Number of VSWT in the wind power plant
$t_{stab}$	Stabilization time
$B$	Bias factor
$D_{eq}$	Equivalent damping factor of the power system
$H_{eq}$	Equivalent inertia constant of the power system
$H_m$	Inertia constant of generating unit $m$
$N$	Number of interconnected areas
$P_{cmd}$	Commanded power of the VSWT
$P_{MPPT}$	Maximum power point tracking of the VSWT
$P_{mt}$	Mechanical power of the VSWT
$S_B$	Rated power of the power system
$S_{B,m}$	Rated power of generating unit $m$
$S_n$	Rated power of a VSWT
$T_{i,j}$	synchronizing moment coefficient of a tie-line between areas $i$ and $j$
$V_W$	Wind speed
$\beta$	Pitch angle
$\Delta f$	Frequency excursion
$\Delta f_{lim}$	Value at which frequency controller of the VSWT activates
$\Delta P_g$	Variation of active power of the power system
$\Delta P_L$	Variation of power demand
$\Delta P_{OP}$	Additional active power in overproduction operation mode
$\Delta P_{tie,i,j}^P$	Tie-line power changed between areas $i$ and $j$
$\Delta P_{tie,i,j}^{P-P}$	Peak-to-peak tie-line power changed between areas $i$ and $j$
$\Delta P_{WF}$	Variation of active power of the wind power plant
$\Omega_{WT}$	Rotational speed of the VSWT
$\Omega_{WT,min}$	Minimum rotational speed of the VSWT
$\Omega_{MPPT}$	Rotational speed at maximum power point tracking

## References

1. Li, D.Y.; Li, P.; Cai, W.C.; Song, Y.D.; Chen, H.J. Adaptive Fault Tolerant Control of Wind Turbines with Guaranteed Transient Performance Considering Active Power Control of Wind Farms. *IEEE Trans. Ind. Electron.* **2017**, *65*, 3275–3285. [[CrossRef](#)]
2. Rasolomampionona, D. A modified power system model for AGC analysis. In Proceedings of the 2009 IEEE Bucharest PowerTech, Bucharest, Romania, 28 June–2 July 2009; pp. 1–6.
3. Du, P.; Matevosyan, J. Forecast system inertia condition and its impact to integrate more renewables. *IEEE Trans. Smart Grid* **2018**, *9*, 1531–1533. [[CrossRef](#)]
4. Toulabi, M.; Bahrami, S.; Ranjbar, A.M. Application of Edge theorem for robust stability analysis of a power system with participating wind power plants in automatic generation control task. *IET Renew. Power Gener.* **2017**, *11*, 1049–1057. [[CrossRef](#)]
5. Toulabi, M.; Bahrami, S.; Ranjbar, A.M. An Input-to-State Stability Approach to Inertial Frequency Response Analysis of Doubly-Fed Induction Generator-Based Wind Turbines. *IEEE Trans. Energy Convers.* **2017**, *32*, 1418–1431. [[CrossRef](#)]
6. Ochoa, D.; Martinez, S. Frequency dependent strategy for mitigating wind power fluctuations of a doubly-fed induction generator wind turbine based on virtual inertia control and blade pitch angle regulation. *Renew. Energy* **2018**, *128*, 108–124. [[CrossRef](#)]
7. Ochoa, D.; Martinez, S. Proposals for Enhancing Frequency Control in Weak and Isolated Power Systems: Application to the Wind-Diesel Power System of San Cristobal Island-Ecuador. *Energies* **2018**, *11*, 910.10.3390/en11040910. [[CrossRef](#)]
8. Bao, Y.; Xu, J.; Liao, S.; Sun, Y.; Li, X.; Jiang, Y.; Ke, D.; Yang, J.; Peng, X. Field Verification of Frequency Control by Energy-Intensive Loads for Isolated Power Systems with High Penetration of Wind Power. *IEEE Trans. Power Syst.* **2018**, in press. [[CrossRef](#)]
9. Fini, M.H.; Golshan, M.E.H. Determining optimal virtual inertia and frequency control parameters to preserve the frequency stability in islanded microgrids with high penetration of renewables. *Electr. Power Syst. Res.* **2018**, *154*, 13–22. [[CrossRef](#)]
10. Li, H.; Wang, X.; Xiao, J. Differential Evolution-Based Load Frequency Robust Control for Micro-Grids with Energy Storage Systems. *Energies* **2018**, *11*, 686. [[CrossRef](#)]
11. Huang, L.; Xin, H.; Zhang, L.; Wang, Z.; Wu, K.; Wang, H. Synchronization and Frequency Regulation of DFIG-Based Wind Turbine Generators With Synchronized Control. *IEEE Trans. Energy Convers.* **2017**, *32*, 1251–1262. [[CrossRef](#)]
12. Luo, X.; Wang, J.; Dooner, M.; Clarke, J. Overview of current development in electrical energy storage technologies and the application potential in power system operation. *Appl. Energy* **2015**, *137*, 511–536. [[CrossRef](#)]
13. Xue, Y.; Tai, N. Review of contribution to frequency control through variable speed wind turbine. *Renew. Energy* **2011**, *36*, 1671–1677.
14. Sun, D.; Sun, L.; Wu, F.; Zu, G. Frequency Inertia Response Control of SCESS-DFIG under Fluctuating Wind Speeds Based on Extended State Observers. *Energies* **2018**, *11*, 830. [[CrossRef](#)]
15. Tavakoli, M.; Pouresmaeil, E.; Adabi, J.; Godina, R.; Catalao, J.P. Load-frequency control in a multi-source power system connected to wind farms through multi terminal HVDC systems. *Comput. Oper. Res.* **2018**, *96*, 305–315. [[CrossRef](#)]
16. Saeed Uz Zaman, M.; Bukhari, S.B.A.; Hazazi, K.M.; Haider, Z.M.; Haider, R.; Kim, C.H. Frequency Response Analysis of a Single-Area Power System with a Modified LFC Model Considering Demand Response and Virtual Inertia. *Energies* **2018**, *11*, 787. [[CrossRef](#)]
17. Sun, Y.; Zhang, Z.; Li, G.; Lin, J. Review on frequency control of power systems with wind power penetration. In Proceedings of the 2010 IEEE International Conference on Power System Technology (POWERCON), Hangzhou, China, 24–28 October 2010; pp. 1–8.
18. Gonzalez-Longatt, F.M.; Bonfiglio, A.; Procopio, R.; Verduci, B. Evaluation of inertial response controllers for full-rated power converter wind turbine (Type 4). In Proceedings of the 2016 IEEE Power and Energy Society General Meeting (PESGM), Boston, MA, USA, 17–21 July 2016; pp. 1–5.
19. Wu, Z.; Gao, W.; Gao, T.; Yan, W.; Zhang, H.; Yan, S.; Wang, X. State-of-the-art review on frequency response of wind power plants in power systems. *J. Modern Power Syst. Clean Energy* **2018**, *6*, 1–16. [[CrossRef](#)]

20. Keung, P.K.; Li, P.; Banakar, H.; Ooi, B.T. Kinetic energy of wind-turbine generators for system frequency support. *IEEE Trans. Power Syst.* **2009**, *24*, 279–287. [[CrossRef](#)]
21. El Itani, S.; Annakkage, U.D.; Joos, G. Short-term frequency support utilizing inertial response of DFIG wind turbines. In Proceedings of the 2011 IEEE Power and Energy Society General Meeting, Detroit, MI, USA, 24–28 July 2011; pp. 1–8.
22. Hansen, A.D.; Altin, M.; Margaris, I.D.; Iov, F.; Tarnowski, G.C. Analysis of the short-term overproduction capability of variable speed wind turbines. *Renew. Energy* **2014**, *68*, 326–336. [[CrossRef](#)]
23. Hafiz, F.; Abdennour, A. Optimal use of kinetic energy for the inertial support from variable speed wind turbines. *Renew. Energy* **2015**, *80*, 629–643. [[CrossRef](#)]
24. Kang, M.; Kim, K.; Muljadi, E.; Park, J.W.; Kang, Y.C. Frequency control support of a doubly-fed induction generator based on the torque limit. *IEEE Trans. Power Syst.* **2016**, *31*, 4575–4583. [[CrossRef](#)]
25. Fernández-Guillamón, A.; Villena-Lapaz, J.; Viguera-Rodríguez, A.; García-Sánchez, T.; Molina-García, Á. An Adaptive Frequency Strategy for Variable Speed Wind Turbines: Application to High Wind Integration into Power Systems. *Energies* **2018**, *11*, 1436. [[CrossRef](#)]
26. Margaris, I.D.; Papathanassiou, S.A.; Hatziaargyriou, N.D.; Hansen, A.D.; Sorensen, P. Frequency control in autonomous power systems with high wind power penetration. *IEEE Trans. Sustain. Energy* **2012**, *3*, 189–199. [[CrossRef](#)]
27. Vidyanandan, K.; Senroy, N. Primary frequency regulation by deloaded wind turbines using variable droop. *IEEE Trans. Power Syst.* **2013**, *28*, 837–846. [[CrossRef](#)]
28. Alsharafi, A.S.; Besheer, A.H.; Emara, H.M. Primary Frequency Response Enhancement for Future Low Inertia Power Systems Using Hybrid Control Technique. *Energies* **2018**, *11*, 699. [[CrossRef](#)]
29. Tielens, P.; Van Hertem, D. Receding horizon control of wind power to provide frequency regulation. *IEEE Trans. Power Syst.* **2017**, *32*, 2663–2672. [[CrossRef](#)]
30. Sahu, R.K.; Gorripotu, T.S.; Panda, S. Automatic generation control of multi-area power systems with diverse energy sources using teaching learning based optimization algorithm. *Eng. Sci. Technol. Int. J.* **2016**, *19*, 113–134. [[CrossRef](#)]
31. Shayeghi, H.; Shayanfar, H.; Jalili, A. Load frequency control strategies: A state-of-the-art survey for the researcher. *Energy Convers. Manag.* **2009**, *50*, 344–353. [[CrossRef](#)]
32. Parmar, K.S.; Majhi, S.; Kothari, D. LFC of an interconnected power system with multi-source power generation in deregulated power environment. *Int. J. Electr. Power Energy Syst.* **2014**, *57*, 277–286. [[CrossRef](#)]
33. Shankar, R.; Chatterjee, K.; Bhushan, R. Impact of energy storage system on load frequency control for diverse sources of interconnected power system in deregulated power environment. *Int. J. Electr. Power Energy Syst.* **2016**, *79*, 11–26. [[CrossRef](#)]
34. Barisal, A. Comparative performance analysis of teaching learning based optimization for automatic load frequency control of multi-source power systems. *Int. J. Electr. Power Energy Syst.* **2015**, *66*, 67–77. [[CrossRef](#)]
35. Sahu, R.K.; Panda, S.; Sekhar, G.C. A novel hybrid PSO-PS optimized fuzzy PI controller for AGC in multi area interconnected power systems. *Int. J. Electr. Power Energy Syst.* **2015**, *64*, 880–893. [[CrossRef](#)]
36. Guha, D.; Roy, P.K.; Banerjee, S. Load frequency control of interconnected power system using grey wolf optimization. *Swarm Evol. Comput.* **2016**, *27*, 97–115. [[CrossRef](#)]
37. Ozdemir, M.T.; Ozturk, D. Comparative Performance Analysis of Optimal PID Parameters Tuning Based on the Optics Inspired Optimization Methods for Automatic Generation Control. *Energies* **2017**, *10*, 2134. [[CrossRef](#)]
38. Mohanty, B.; Panda, S.; Hota, P. Controller parameters tuning of differential evolution algorithm and its application to load frequency control of multi-source power system. *Int. J. Electr. Power Energy Syst.* **2014**, *54*, 77–85. [[CrossRef](#)]
39. Zare, K.; Hagh, M.T.; Morsali, J. Effective oscillation damping of an interconnected multi-source power system with automatic generation control and TCSC. *Int. J. Electr. Power Energy Syst.* **2015**, *65*, 220–230. [[CrossRef](#)]
40. Gorripotu, T.S.; Sahu, R.K.; Panda, S. AGC of a multi-area power system under deregulated environment using redox flow batteries and interline power flow controller. *Eng. Sci. Technol. Int. J.* **2015**, *18*, 555–578. [[CrossRef](#)]
41. Hota, P.; Mohanty, B. Automatic generation control of multi source power generation under deregulated environment. *Int. J. Electr. Power Energy Syst.* **2016**, *75*, 205–214. [[CrossRef](#)]

42. Ketabi, A.; Fini, M.H. An underfrequency load shedding scheme for hybrid and multiarea power systems. *IEEE Trans. Smart Grid* **2015**, *6*, 82–91. [[CrossRef](#)]
43. Mi, Y.; Fu, Y.; Li, D.; Wang, C.; Loh, P.C.; Wang, P. The sliding mode load frequency control for hybrid power system based on disturbance observer. *Int. J. Electr. Power Energy Syst.* **2016**, *74*, 446–452. [[CrossRef](#)]
44. Kerdphol, T.; Rahman, F.S.; Mitani, Y. Virtual Inertia Control Application to Enhance Frequency Stability of Interconnected Power Systems with High Renewable Energy Penetration. *Energies* **2018**, *11*, 981. [[CrossRef](#)]
45. Babahajiani, P.; Shafiee, Q.; Bevrani, H. Intelligent demand response contribution in frequency control of multi-area power systems. *IEEE Trans. Smart Grid* **2018**, *9*, 1282–1291. [[CrossRef](#)]
46. 2030 Energy Strategy. Available online: <https://ec.europa.eu/energy/en/topics/energy-strategy-and-energy-union/2030-energy-strategy> (accessed on 15 August 2018).
47. Dreidy, M.; Mokhlis, H.; Mekhilef, S. Inertia response and frequency control techniques for renewable energy sources: A review. *Renew. Sustain. Energy Rev.* **2017**, *69*, 144–155. [[CrossRef](#)]
48. Wang, H.; Yang, J.; Chen, Z.; Ge, W.; Hu, S.; Ma, Y.; Li, Y.; Zhang, G.; Yang, L. Gain Scheduled Torque Compensation of PMSG-Based Wind Turbine for Frequency Regulation in an Isolated Grid. *Energies* **2018**, *11*, 1623. [[CrossRef](#)]
49. Jallad, J.; Mekhilef, S.; Mokhlis, H. Frequency Regulation Strategies in Grid Integrated Offshore Wind Turbines via VSC-HVDC Technology: A Review. *Energies* **2017**, *10*, 1244. [[CrossRef](#)]
50. Tavakkoli, M.; Adabi, J.; Zabihi, S.; Godina, R.; Pouresmaeil, E. Reserve Allocation of Photovoltaic Systems to Improve Frequency Stability in Hybrid Power Systems. *Energies* **2018**, *11*, 583. [[CrossRef](#)]
51. Kayikçi, M.; Milanovic, J.V. Dynamic contribution of DFIG-based wind plants to system frequency disturbances. *IEEE Trans. Power Syst.* **2009**, *24*, 859–867. [[CrossRef](#)]
52. Morren, J.; de Haan, S.W.H.; Kling, W.L.; Ferreira, J.A. Wind turbines emulating inertia and supporting primary frequency control. *IEEE Trans. Power Syst.* **2006**, *21*, 433–434. [[CrossRef](#)]
53. Ramtharan, G.; Jenkins, N.; Ekanayake, J. Frequency support from doubly fed induction generator wind turbines. *IET Renew. Power Gener.* **2007**, *1*, 3–9. [[CrossRef](#)]
54. Chowdhury, B.H.; Ma, H.T. Frequency regulation with wind power plants. In Proceedings of the 2008 IEEE Power and Energy Society General Meeting—Conversion and Delivery of Electrical Energy in the 21st Century, 20–24 July 2008; pp. 1–5.
55. Conroy, J.F.; Watson, R. Frequency response capability of full converter wind turbine generators in comparison to conventional generation. *IEEE Trans. Power Syst.* **2008**, *23*, 649–656. [[CrossRef](#)]
56. Mauricio, J.M.; Marano, A.; Gómez-Expósito, A.; Ramos, J.L.M. Frequency regulation contribution through variable-speed wind energy conversion systems. *IEEE Trans. Power Syst.* **2009**, *24*, 173–180. [[CrossRef](#)]
57. Bassi, F.; Caciolli, L.; Giannuzzi, G.; Corsi, N.; Giorgi, A. Use of hidden inertia from wind generation for frequency support in power grids. In Proceedings of the 2016 IEEE AEIT International Annual Conference (AEIT), Capri, Italy, 5–7 October 2016; pp. 1–6.
58. Gonzalez-Longatt, F.M. Impact of emulated inertia from wind power on under-frequency protection schemes of future power systems. *J. Modern Power Syst. Clean Energy* **2016**, *4*, 211–218. [[CrossRef](#)]
59. Hu, J.; Sun, L.; Yuan, X.; Wang, S.; Chi, Y. Modeling of type 3 wind turbines with df/dt inertia control for system frequency response study. *IEEE Trans. Power Syst.* **2017**, *32*, 2799–2809. [[CrossRef](#)]
60. Bonfiglio, A.; Invernizzi, M.; Labella, A.; Procopio, R. Design and Implementation of a Variable Synthetic Inertia Controller for Wind Generating Units. *IEEE Trans. Power Syst.* **2018**, in press.
61. Tarnowski, G.C.; Kjar, P.C.; Sorensen, P.E.; Ostergaard, J. Variable speed wind turbines capability for temporary over-production. In Proceedings of the 2009 IEEE Power & Energy Society General Meeting (PES'09), Calgary, AB, Canada, 26–30 July 2009; pp. 1–7.
62. Kundur, P.; Balu, N.J.; Lauby, M.G. *Power System Stability and Control*; McGraw-Hill: New York, NY, USA, 1994; Volume 7.
63. Tan, W. Load frequency control: Problems and solutions. In Proceedings of the 2011 IEEE 30th Chinese Control Conference (CCC), Yantai, China, 22–24 July 2011; pp. 6281–6286.
64. Ma, M.; Chen, H.; Liu, X.; Allgöwer, F. Distributed model predictive load frequency control of multi-area interconnected power system. *Int. J. Electr. Power Energy Syst.* **2014**, *62*, 289–298. [[CrossRef](#)]
65. Yousef, H.A.; Khalfan, A.K.; Albadi, M.H.; Hosseinzadeh, N. Load frequency control of a multi-area power system: An adaptive fuzzy logic approach. *IEEE Trans. Power Syst.* **2014**, *29*, 1822–1830. [[CrossRef](#)]

66. Pan, I.; Das, S. Fractional-order load-frequency control of interconnected power systems using chaotic multi-objective optimization. *Appl. Soft Comput.* **2015**, *29*, 328–344. [[CrossRef](#)]
67. Sathya, M.; Ansari, M.M.T. Load frequency control using Bat inspired algorithm based dual mode gain scheduling of PI controllers for interconnected power system. *Int. J. Electr. Power Energy Syst.* **2015**, *64*, 365–374. [[CrossRef](#)]
68. Abdelaziz, A.; Ali, E. Cuckoo search algorithm based load frequency controller design for nonlinear interconnected power system. *Int. J. Electr. Power Energy Syst.* **2015**, *73*, 632–643. [[CrossRef](#)]
69. Padhan, D.G.; Majhi, S. A new control scheme for PID load frequency controller of single-area and multi-area power systems. *ISA Trans.* **2013**, *52*, 242–251. [[CrossRef](#)] [[PubMed](#)]
70. Chang, Y.; Liu, R.; Ba, Y.; Li, W. A New Control Logic for a Wind-Area on the Balancing Authority Area Control Error Limit Standard for Load Frequency Control. *Energies* **2018**, *11*, 121. [[CrossRef](#)]
71. Pyller, M.; Achilles, S. Aggregated wind park models for analyzing power system dynamics. In Proceedings of the 4th International Workshop Large-Scale Integration of Wind Power and Transmission Networks, Billund, Denmark, 20–21 October 2003.
72. Mokhtari, M.; Aminifar, F. Toward wide-area oscillation control through doubly-fed induction generator wind farms. *IEEE Trans. Power Syst.* **2014**, *29*, 2985–2992. [[CrossRef](#)]
73. Miller, N.W.; Sanchez-Gasca, J.J.; Price, W.W.; Delmerico, R.W. Dynamic modeling of GE 1.5 and 3.6 MW wind turbine-generators for stability simulations. In Proceedings of the 2003 IEEE Power Engineering Society General Meeting, Toronto, ON, Canada, 13–17 July 2003; Volume 3, pp. 1977–1983.
74. Ullah, N.R.; Thiringer, T.; Karlsson, D. Temporary primary frequency control support by variable speed wind turbines—Potential and applications. *IEEE Trans. Power Syst.* **2008**, *23*, 601–612. [[CrossRef](#)]
75. Baccino, F.; Conte, F.; Grillo, S.; Massucco, S.; Silvestro, F. An optimal model-based control technique to improve wind farm participation to frequency regulation. *IEEE Trans. Sustain. Energy* **2015**, *6*, 993–1003. [[CrossRef](#)]
76. Zhao, J.; Lyu, X.; Fu, Y.; Hu, X.; Li, F. Coordinated microgrid frequency regulation based on DFIG variable coefficient using virtual inertia and primary frequency control. *IEEE Trans. Energy Convers.* **2016**, *31*, 833–845. [[CrossRef](#)]
77. Martínez-Lucas, G.; Sarasúa, J.I.; Sánchez-Fernández, J.Á. Frequency Regulation of a Hybrid Wind–Hydro Power Plant in an Isolated Power System. *Energies* **2018**, *11*, 239. [[CrossRef](#)]
78. Perera, A.T.D.; Nik, V.M.; Mauree, D.; Scartezini, J.L. Electrical hubs: An effective way to integrate non-dispatchable renewable energy sources with minimum impact to the grid. *Appl. Energy* **2017**, *190*, 232–248. [[CrossRef](#)]
79. Wind energy in Europe: Scenarios for 2030. *Wind Eur.* **2017**. Available online: <https://windeurope.org/wp-content/uploads/files/about-wind/reports/Wind-energy-in-Europe-Scenarios-for-2030.pdf> (accessed on 10 August 2018).
80. Technology Roadmap: Solar Photovoltaic Energy. *Int. Energy Agency* **2014**. Available online: [https://www.iea.org/publications/freepublications/publication/TechnologyRoadmapSolarPhotovoltaicEnergy\\_2014edition.pdf](https://www.iea.org/publications/freepublications/publication/TechnologyRoadmapSolarPhotovoltaicEnergy_2014edition.pdf) (accessed on 10 August 2018).
81. Huang, C.; Yue, D.; Xie, X.; Xie, J. Anti-windup load frequency controller design for multi-area power system with generation rate constraint. *Energies* **2016**, *9*, 330. [[CrossRef](#)]
82. Zeng, G.Q.; Xie, X.Q.; Chen, M.R. An Adaptive Model Predictive Load Frequency Control Method for Multi-Area Interconnected Power Systems with Photovoltaic Generations. *Energies* **2017**, *10*, 1840. [[CrossRef](#)]
83. Yang, L.; Liu, T.; Hill, D.J. Decentralized periodic event-triggered frequency regulation for multi-area power systems. In Proceedings of the 2018 IEEE Power Systems Computation Conference (PSCC), Dublin, Ireland, 11–15 June 2017; pp. 1–7.
84. Lu, K.; Zhou, W.; Zeng, G.; Zheng, Y. Constrained population extremal optimization-based robust load frequency control of multi-area interconnected power system. *Int. J. Electr. Power Energy Syst.* **2019**, *105*, 249–271. [[CrossRef](#)]
85. Huang, H.; Li, F. Sensitivity analysis of load-damping characteristic in power system frequency regulation. *IEEE Trans. Power Syst.* **2013**, *28*, 1324–1335. [[CrossRef](#)]
86. Tielens, P.; Van Hertem, D. The relevance of inertia in power systems. *Renew. Sustain. Energy Rev.* **2016**, *55*, 999–1009. [[CrossRef](#)]

87. Ali, E.; Abd-Elazim, S. Bacteria foraging optimization algorithm based load frequency controller for interconnected power system. *Int. J. Electr. Power Energy Syst.* **2011**, *33*, 633–638. [[CrossRef](#)]
88. Sudha, K.; Santhi, R.V. Robust decentralized load frequency control of interconnected power system with generation rate constraint using type-2 fuzzy approach. *Int. J. Electr. Power Energy Syst.* **2011**, *33*, 699–707. [[CrossRef](#)]
89. Jiang, L.; Yao, W.; Wu, Q.; Wen, J.; Cheng, S.; others. Delay-dependent stability for load frequency control with constant and time-varying delays. *IEEE Trans. Power Syst.* **2012**, *27*, 932. [[CrossRef](#)]
90. Masuta, T.; Yokoyama, A. Supplementary load frequency control by use of a number of both electric vehicles and heat pump water heaters. *IEEE Trans. Smart Grid* **2012**, *3*, 1253–1262. [[CrossRef](#)]
91. Shabani, H.; Vahidi, B.; Ebrahimpour, M. A robust PID controller based on imperialist competitive algorithm for load-frequency control of power systems. *ISA Trans.* **2013**, *52*, 88–95. [[CrossRef](#)] [[PubMed](#)]
92. Rout, U.K.; Sahu, R.K.; Panda, S. Design and analysis of differential evolution algorithm based automatic generation control for interconnected power system. *Ain Shams Eng. J.* **2013**, *4*, 409–421. [[CrossRef](#)]
93. Sahu, R.K.; Panda, S.; Rout, U.K. DE optimized parallel 2-DOF PID controller for load frequency control of power system with governor dead-band nonlinearity. *Int. J. Electr. Power Energy Syst.* **2013**, *49*, 19–33. [[CrossRef](#)]
94. Ruiz, S.; Patiño, J.; Espinosa, J. Load Frequency Control of a Multi-area Power System Incorporating Variable-speed Wind Turbines. **2016**, in press.
95. Dong, L.; Tang, Y.; He, H.; Sun, C. An event-triggered approach for load frequency control with supplementary ADP. *IEEE Trans. Power Syst.* **2017**, *32*, 581–589. [[CrossRef](#)]
96. Peng, C.; Zhang, J.; Yan, H. Adaptive Event-Triggering  $H_\infty$  Load Frequency Control for Network-Based Power Systems. *IEEE Trans. Ind. Electr.* **2018**, *65*, 1685–1694. [[CrossRef](#)]
97. Wu, Y.; Wei, Z.; Weng, J.; Li, X.; Deng, R.H. Resonance attacks on load frequency control of smart grids. *IEEE Trans. Smart Grid* **2018**, *9*, 4490–4502. [[CrossRef](#)]



© 2018 by the authors. Licensee MDPI, Basel, Switzerland. This article is an open access article distributed under the terms and conditions of the Creative Commons Attribution (CC BY) license (<http://creativecommons.org/licenses/by/4.0/>).